Impacts of Organic Sorbates on Ionic Conductivity and Nanostructure of Perfluorinated Sulfonic-Acid Ionomers

Adlai Katzenberg[1+], Andrea Angulo[1], Ahmet Kusoglu[2*], and Miguel A. Modestino[1*]

[1]Tandon School of Engineering, New York University, Brooklyn, NY 11201

[2]Lawrence Berkeley National Laboratory, Berkeley, CA 94720

[*]akusoglu@lbl.gov, modestino@nyu.edu

Abstract

This study provides insights into structure-property relationships of Nafion membranes swollen with organic sorbates, revealing correlations between sorbate polarity, ionomer domain structure, and ionic conductivity. Swelling, nanostructure, and ionic conductivity of Nafion in the presence of short-chain alcohols and alkanes was studied by infrared spectroscopy, X-ray scattering, and voltammetry. Nafion equilibrated with alkanes exhibited negligible uptake and nanoswelling, while alcohols induced nanoscopic- to macroscopic- swelling ratios that increased with alcohol polarity. In mixed-sorbate environments including organics and water, alcohols preserved the overall ionomer domain structure but altered the matrix to enable higher sorbate uptake. Alkanes did not demonstrably alter the hydrated nanostructure or conductivity. Identifying the impacts of organic sorbates on structure-property relationships in ionomers such as Nafion is imperative as membrane-based electrochemical devices find applications in emerging areas ranging from organic fuel cells to the synthesis of fuels and chemicals.

Introduction

Perfluorinated sulfonic acid membranes (PFSAs) have enabled substantial performance enhancements and cost reductions in electrochemical energy conversion systems such as proton exchange membrane (PEM) hydrogen fuel cells, redox-flow batteries, and water electrolyzers by playing a dual role as a separator and ion-conducting media that prevents crossover of chemical species between the cathodic and anodic sites while providing a low-resistance pathway for proton transport[1–4]. Ionic conductivity in PFSAs is intimately related to their nanostructured morphology dictated by phase separation between a hydrophobic fluoropolymer matrix and acidic side-chains. This nanostructure is highly sensitive to environmental conditions; most critically, external water drives formation and hydration of acid-rich clusters which swell and percolate into an interconnected hydrated ionomer network[5]. The relationships between hydration, nanostructure, and key transport properties including conductivity, water transport, gas permeability, and mechanical strength in PFSAs have been investigated rigorously for decades and are highly relevant for the aqueous electrochemical systems in which they have historically been employed[1,2,6,7].

The advantages afforded by ionomer membranes in hydrogen fuel cells and water electrolyzers have been extended to CO_2 electrolysis[8–11], direct-methanol fuel cells (DMFCs)[12–14], electro-organic synthesis[15–17], and electrochemical swing absorbers[18]. These devices expose membranes to more complex chemical environments (*i.e.*, multiple organic and inorganic chemical species) than a fuel cell or water electrolyzer, which interact with and impact the PFSAs structure and transport properties. Motivated by the need to understand structure-property relationships of ion-conducting membranes in the presence of organic chemical species, this study explores the effects of organic sorbates ranging from polar alcohols to nonpolar alkanes on the swelling, ionomer nanostructure and ionic conductivity of Nafion™ membranes. The results reveal that both macroscopic and nanoscopic swelling are strongly dependent on sorbate polarity, with a large but poorly-defined ionomer domain-network in alcohol-saturated Nafion leading to low ionic conductivity despite high sorbate uptake. These changes in the ionomer phase separation persist with the introduction of water in the presence of organic sorbates, leading to unique solvent-structure-property

relationships that differ from the well-understood water-Nafion relationships. The insights of this study will help guide the development and implementation of ionomers for emerging organic electrochemical devices.

Results and Discussion

Ion transport in Nafion emerges due to complex multiscale physicochemical interactions between water and the fluoropolymer. In hydrated Nafion, water solvates sulfonic acid groups, dissociating protons as mobile charge carriers. The geometry of the ionomer domains is determined by a balance between water sorption in the hydrophilic regions opposed by deformation of the fluoropolymer matrix during swelling[2,19]. Macroscopic PFSA conductivity is highly sensitive to water content as both the morphology of ionomer domains and the concentration/mobility of ions within those domains are linked to hydration levels. Both of these factors are expected to change when Nafion is swollen with organic species; size and polarity of the sorbing species have been shown to impact bulk swelling (and likely the ionomer domain structure)[20–25] and the polarity, pKa, and viscosity would impact the concentration and mobility of protons.

Figure 1 shows the ionic conductivity of Nafion membrane vapor-equilibrated with water (black squares), methanol (teal triangles), ethanol (orange circles), isopropanol (purple diamonds) and octane (yellow hexagrams) from the vapor phase. For all alcohols, Nafion showed nonlinear scaling of ionic conductivity with increasing concentration of sorbate in the vapor phase; a trend consistent with the impact of water uptake on PFSA ionic conductivity. On the other hand, Nafion showed minimal sorbate uptake and negligible ionic conductivity when exposed to vapor of nonpolar alkanes (see Table S1 in the supporting information for uptake data). For the alcohols studied, the maximum sorbate volume fraction (ϕ_{max}) increased with decreasing solvent polarity ($\phi_{max,\ water} < \phi_{max,\ MeOH} < \phi_{max,\ EtOH} < \phi_{max,\ iPrOH}$), opposite of the molar solvent uptake (Table S1, supporting information). This is consistent with prior literature[21,26–28] and attributed to the balance between solvent/solute interaction energy (more favorable for more polar solvents) and mechanical deformation induced by swelling, leading to small molar uptake but large volume expansion for large solutes like iPrOH. Alcohols can also plasticize the fluoropolymer matrix enabling higher swelling ratios than water swollen membranes[29]. Conductivity at a given solvent volume fraction, however, scaled

with solvent polarity ($\kappa_{water} > \kappa_{MeOH} > \kappa_{EtOH} > \kappa_{iPrOH}$). This is consistent with consideration of each solute as a mobile electrolyte phase within the ionomer domains, with conductivity given by $\kappa = nFC_{H^+}\mu_{H^+}$ where n is the charge of a proton, F is Faraday's constant, C_{H^+} is the proton concentration, and μ_{H^+} the proton mobility. Saito et al. demonstrated that μ_{H^+} is the dominant factor in determining ionomer ionic conductivity and decreased logarithmically with alkyl chain length for Nafion swollen with alcohols[21]. However, this scaling is complicated by morphological considerations in PFSAs where solvent uptake plays a critical role in the percolation of ion-conducting domains, and where for a given sorbate the PFSA ionic conductivity generally increases with the volume fraction of mobile phase.

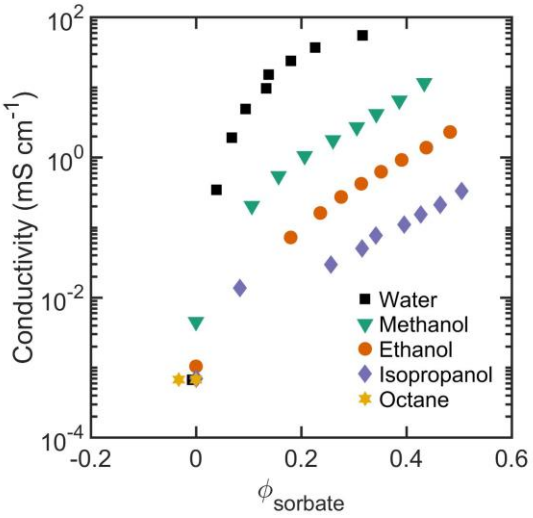

Figure 1: Conductivity (mS cm^{-1}) of Nafion at room temperature equilibrated with water (black squares), alcohols (methanol, ethanol, and isopropanol; teal triangles, orange circles, and purple diamonds, respectively), and octane (yellow hexagrams) from vapor phase. Conductivity scaled not only with sorbate volume fraction but with polarity and molar volume of sorbate.

The decreasing conductivity of Nafion with increased sorbate volume fraction could be attributed to the interplay of the mobility and concentration of protons in each of these sorbates, as well as distinct changes in the ionomer morphology when swollen with alcohols rather than water. In general, hydrated Nafion exhibits a morphology characterized by locally flat and highly branched water-rich domains embedded in a fluoropolymer matrix[5,30–33]. This morphology has been widely studied by small-angle X-ray scattering (SAXS) which reveals a broad scattering peak attributed to water-rich domains around scattering vector q of 0.15 Å^{-1} or domain spacing ($d_{space} = 2\pi/q$) between 3 and 6 nm[34–40]. Figure 2 shows Nafion's

SAXS profiles under dry environments and equilibrated with liquid water, methanol, ethanol, isopropanol, hexane, heptane, and octane. Alkanes induced minimal change in the scattering profiles, consistent with their negligible bulk uptake. Alcohol-swollen Nafion, however, exhibited significant changes in the scattering behavior; the ionomer peak shifted to lower q values relative to the dry material, indicating ionomer domain swelling, but with broader peaks than water-swollen Nafion. There was also a clear shift to larger q (smaller d_{space}) with increasing alcohol size. While alkane-saturated Nafion showed similar d_{space} and full-width at half maximum (*FWHM)* to the dry material, these features scaled with sorbate polarity in the case of alcohol-saturated Nafion; increasing polarity coincided with increased d_{space} and lower *FWHM* (see Figure S4 in the supporting information). Less polar alcohols appeared to result in smaller ionomer nano-domains within a network of increasing spatial disorder, contributing to the reduction in ionic conductivity despite high alcohol volume fraction. It is also important to note that the matrix knee (q ~ 0.05 $Å^{-1}$), arising from the ordered distribution of PTFE crystallites within the fluoropolymer matrix, is absent in the alcohol-swollen Nafion (Figure 2). Alcohols, while interacting more preferably with the fluoropolymer matrix compared to water, are still not able to dissolve PTFE crystallites, so this loss of scattering is likely due to redistribution (*i.e.*, increasing isotropy) of crystallites within the ionomer's amorphous matrix, which is consistent with observations in acetone-swollen Nafion[22], and with matrix plasticization observed in methanol-swollen Nafion[29].

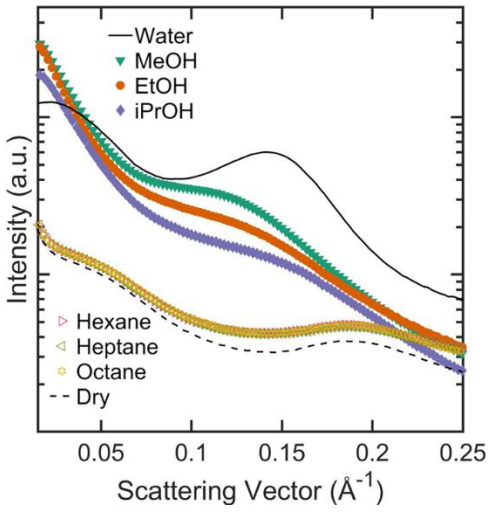

Figure 2: (a) SAXS profiles of Nafion 117 dry and equilibrated with various liquid sorbates. Alkanes induced little change in the scattering profiles, consistent with their minimal mass uptake. Alcohols induced a strong shift in the ionomer peak to lower scattering vectors while increasing its breadth and decreasing its intensity relative to water-equilibrated Nafion.

Changes in nanostructure morphology are also clear when comparing the ionomer nano-domain swelling ($d_{saturated}$ / d_{dry}) to bulk swelling for the different species (Figure 3a). In water-swollen Nafion, there is a well-established correlation between nanoswelling and water volume fraction:

$$\frac{d}{d_{dry}} = (1 - \phi_{water})^{-m} = (\phi_p)^{-m} \quad \text{(Equation 1)}$$

where m is a constant that indicates the shape/morphology of ionomer domains[2,19]. For Nafion swollen with water ($\phi_p > 0.5$), m is slightly greater than 1 indicating a locally lamellar domain structure with mesoscale connectivity, while in dispersion ($\phi_p < 0.5$), m approaches 0.5 reflecting cylindrical polymer aggregates[30,34,41,42]. Figure 3a shows that organic sorbates deviated significantly from water-Nafion behavior with nanoswelling related to sorbate polarity. Alkanes induced almost no nanoswelling in Nafion, confirming limited penetration of nonpolar sorbates into ionomer domains. Alcohols did cause substantial nanoswelling in Nafion with magnitude decreasing monotonically with increasing sorbate volume fraction (*i.e.*, methanol > ethanol > isopropanol). This indicates that the distribution of sorbate within the ionomer structure is impacted by sorbate chemical identity, as in the absence of structural changes the nanoswelling would scale identically with sorbate volume fraction regardless of the sorbate identity. Figure 3b shows the morphological exponent *m* was strongly correlated to sorbate polarity (represented as dielectric constant) and shifted towards lower values (indicating loss of lamellar structure and transition towards dispersion-like scaling) with decreasing polarity. It should be noted the m values reported here are based only on dry and sorbate-saturated Nafion. Without intermediate swelling fractions, the relationship in Equation 1 cannot be precisely determined. Still, the trend clearly shows a correlation between solvent polarity and the relationship between bulk and nano-domain swelling through morphological rearrangements.

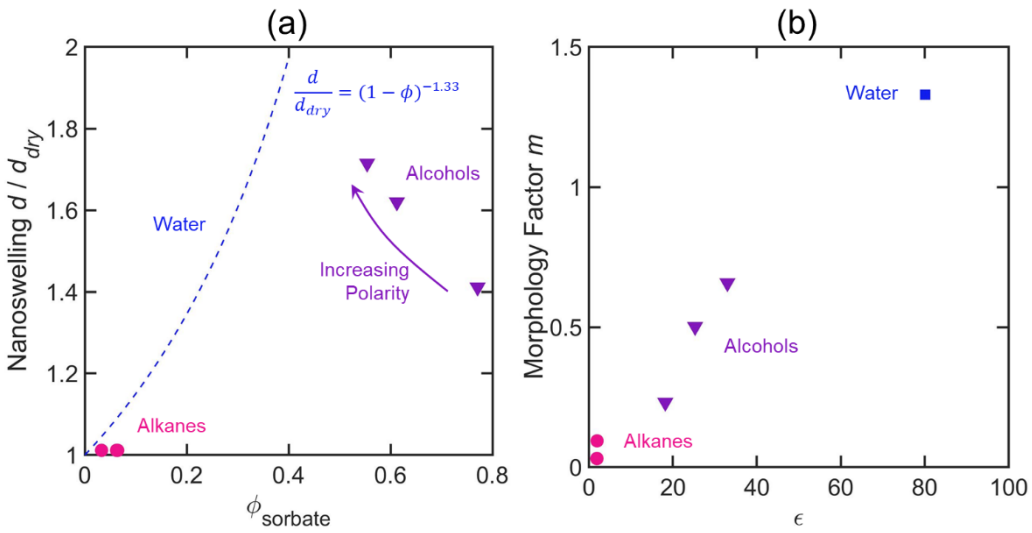

Figure 3: (a) Nanoswelling/macroscopic swelling relationships for Nafion swollen with organic species deviated significantly from water-swollen Nafion. (b) The nanoscale morphology factor *m* increased monotonically with solvent dielectric constant.

These changes likely arise from the affinity of the sorbate for different moieties in the polymer; highly polar water molecules ($\epsilon \sim 80$) strongly solvate sulfonic acid moieties but display minimal affinity for perfluoroether side chains, resulting in strong phase separation and a relatively sharp fluoropolymer/water interface. Alcohols and acetone have been shown to interact with the perfluoroether side chains, partition across the water-fluoropolymer interface, and impact the fluoropolymer matrix[21,22,29,43,44]. Increased mixing of sorbate and fluoropolymer would have the following impacts on ionomer domain structure and conductivity: (*i*) reduced phase separation and redistribution of sorbate across the liquid/fluoropolymer interface, (*ii*) significant changes in the shape and ordering of ionomer domains accompanied by disruption of the domain-network, and (*iii*) increased penetration of fluoropolymer into swollen ionomer channels. Together, these effects would result in increased network tortuosity (per structural changes), increased local viscosity within ionomer channels, and decreased H^+ mobility despite higher fraction of the mobile phase.

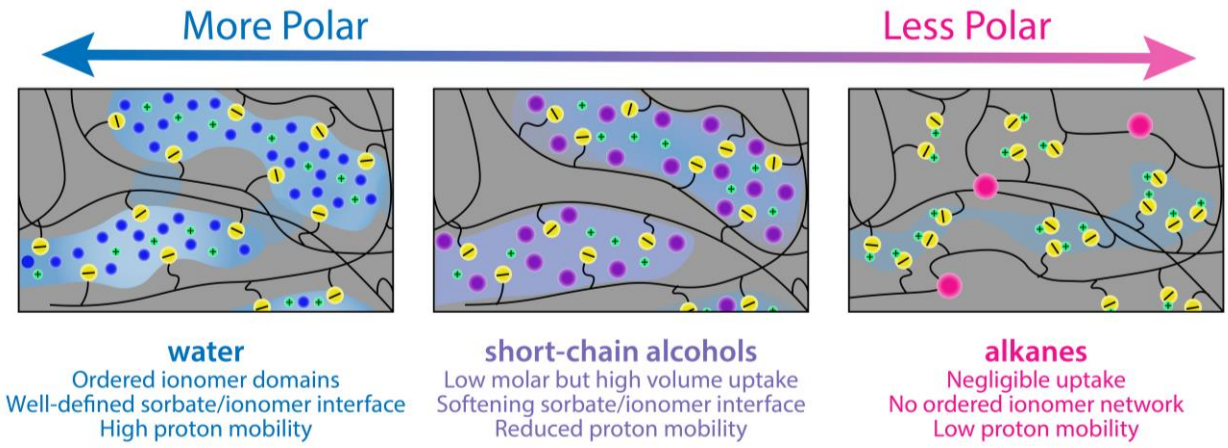

Figure 4: Overview of the proposed impacts of sorbate polarity on ionomer structure and transport. Water strongly solvates protons and sulfonic acid groups while displaying minimal affinity for perfluoroether side chains or fluoropolymer backbone. This produces a sharp fluoropolymer/ionomer interface with a high concentration of mobile protons. Alcohols of increasing size (decreasing polarity) increasingly mix with perfluoroether side chains, softening the fluoropolymer/sorbate interface and decreasing proton mobility due in part to increases in local viscosity. Alkanes display minimal affinity for ionic groups and fluoropolymer and do not significantly alter Nafion from its dry state.

While studying the properties of PFSAs in pure sorbate environments is useful in characterizing sorbate/ionomer interactions, organic electrochemical devices commonly employ water as a solvent and/or to maintain membrane hydration[45], and thus it is important to understand of how organic species interact with PFSAs in the presence of water.

The limited uptake of alkanes by Nafion in pure-sorbate studies suggests a mixture of alkane and water vapor will likely lead to similar nano-swelling and ionic conductivity to pure water, while alcohol/water mixtures may exhibit more complex behavior. At a given water saturation, adding alcohol vapor may add mechanical resistance to hydration by further deforming the fluoropolymer matrix, shifting the equilibrium toward lower water concentration. However, these mechanical considerations are complicated by the possible alcohol-induced matrix plasticization and change in domain network morphology. To assess these competing effects, Nafion was exposed to controlled mixtures of water and organic vapor. In these experiments, a water-saturated stream was balanced by an organic vapor-saturated stream. Figure 5(a) shows impact of introduction of organic vapors at a given water saturation on Nafion's conductivity. As expected, alkanes did not significantly impact the water uptake or ionic conductivity of water-swollen Nafion since their penetration was negligible.

Alcohols induced large polarity-related differences in Nafion ionic conductivity at low water content which became increasingly small as water content increased, approaching the water-saturated ionic conductivity. At low water content, the presence of alcohols increased Nafion's ionic conductivity due to the inherent conductivity of alcohol-swollen Nafion, but this improvement was lost at intermediate and high water saturation. Alcohol-driven loss of conductivity at intermediate water content scaled similarly to pure sorbate systems ($\kappa_{water} \sim \kappa_{Water+MeOH} > \kappa_{Water+EtOH} > \kappa_{Water+iPrOH}$) which suggests appreciable uptake of these alcohols in addition to water. Figure 5b shows ionic conductivity of Nafion swollen with organic vapor alone (empty markers) and organic vapor balanced with water vapor (filled markers). It is clear that at intermediate alcohol/water saturation, the conductivity generally fell between that of the pure sorbates (water and alcohol) suggesting both species are absorbed and contribute to the ionic conductivity. In these environments, ion conduction is governed by the same physical considerations as in single-sorbate environments (*i.e.*, the shape and tortuosity of ionomer domains and the mobility and concentration of protons within those domains). Similar observations were recently reported for cation-exchanged PFSI; Cerium doping was shown to impact ionomer conductivity by reducing proton concentration and mobility as well as increasing tortuosity of the overall domain structure[46]. Mixed ionomer-sorbate systems may exhibit additional complexity due to the unknown composition of the sorbate mixture inside the ionomer domains.

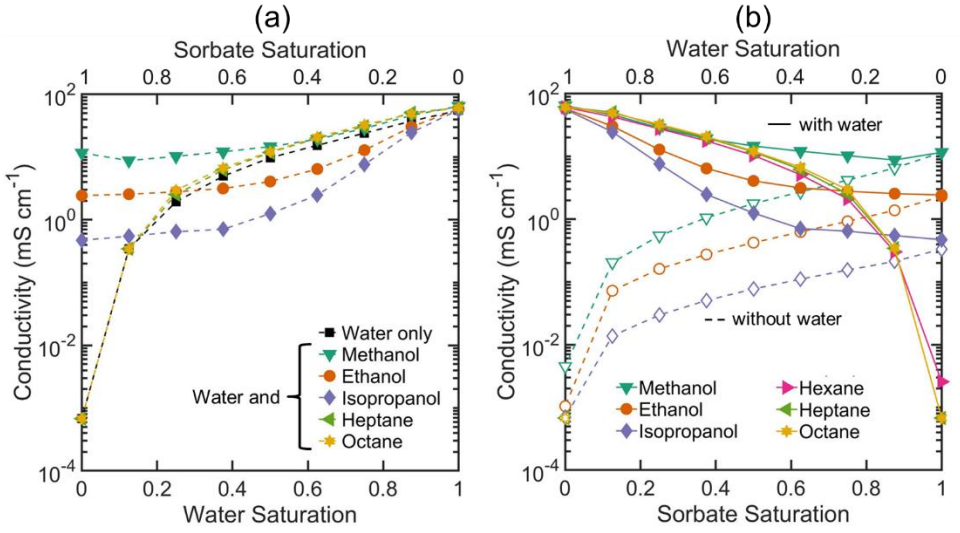

Figure 5: (a) Ionic conductivity of Nafion swollen with water alone (black squares) and with various organic species. While nonpolar alkanes had minimal impact on the ionic conductivity, alcohols imparted high conductivity at low water saturation (high organic saturation) but approached the conductivity of water-swollen Nafion at higher water saturation (low organic saturation). (b) Ionic conductivity of Nafion swollen with organics alone (empty markers) and organic vapor balanced with water vapor (filled markers). Ionic conductivity of alcohol- and water- swollen Nafion was generally between that of the pure sorbate cases, indicated uptake and influence of both species on the ionomer conductivity.

Sorbate mixture composition was quantitatively determined by ATR-FTIR using a linear regression trained with water-saturated and organic-saturated Nafion FTIR spectra to determine the relative contributions of each sorbate. Figure 6 shows sorbate uptake isotherms of alcohol in Nafion in mixed- and single- sorbate environments, with consistently higher alcohol uptake in Nafion with the presence of water. This complementary behavior points to differences in how the chemical species interact with and swell Nafion; swelling in Nafion at a given water activity is generally constrained by the fluoropolymer resistance to mechanical deformation. As observed in pure-sorbate environments, alcohols may interact with the perfluoroether chains and soften the water/fluoropolymer interface while reducing the matrix stress and allowing for higher total sorbate uptake than in a single-sorbate environment at the same chemical activity. Alcohols can benefit from this by mixing with water in the ionomer regions and by partitioning across the water/fluoropolymer interface. This would result in increased total swelling and possibly a non-uniform distribution of alcohol and water within the ionomer domain structure. This possible distribution of sorbates is also consistent with ionic conductivity results for mixed-sorbate Nafion which show conductivity higher than alcohol alone as water contributes to a higher proton mobility and produces more strongly phase-separated ionomer domains. On the other hand, mixed-sorbate-swollen Nafion conductivity was lower than water-swollen Nafion as alcohols in the ionomer domains increase local viscosity and their partitioning across the water/fluoropolymer interface would alter the domain structure and increase side chain penetration into the water-rich domains.

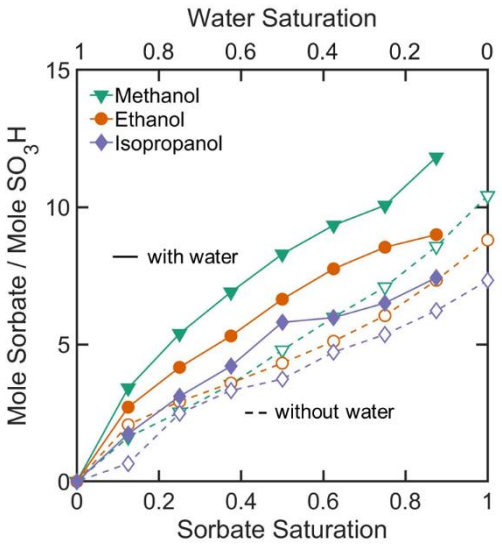

Figure 6: Molar uptake of organic sorbates with water (filled markers, solid lines) and without water (empty markers, dashed lines) determined by regression of ATR-FTIR spectra. Overall, mixed-sorbate systems with alcohol exhibited higher molar uptake than single-sorbate systems, with much of the increase attributed to additional alcohol uptake.

The impacts of mixed-sorbate environments on Nafion's phase-separated nanomorphology were investigated by SAXS of Nafion equilibrated with mixed vapor saturated with water and an organic species. SAXS profiles are shown in Figure 7 and reveal a well-defined ionomer peak with alkane/water mixtures closely resembling the spectra of water-equilibrated Nafion. Negligible uptake of alkanes resulted in similar Nafion nanostructure, swelling, and conductivity to Nafion with water alone. Alcohol/water mixtures show an ionomer peak shifted to lower scattering vector q (larger domain spacing) than water alone and with greater intensity/sharpness than alcohol alone. Increased total sorbate uptake for mixed sorbate systems is expected to produce larger domain spacing, so this does not necessarily indicate a change in the way water/alcohol are partitioned as was observed in the pure sorbates (*i.e.*, no change in m can be resolved). However, the matrix knee is notably absent from isopropanol/water- and ethanol/water Nafion, suggesting the role of the alcohol in altering the distribution of crystallites in pure solvents persists in the presence of water. SAXS profiles suggest that mixed water-alcohol environments preserve the overall domain structure of water-swollen Nafion but with larger interdomain spacing enabled by matrix plasticization, disruption of inter-crystalline order, and/or distribution of alcohol across the water/fluoropolymer interface. Water appears to play a critical role in ionomer network formation, confirming the orders-of-magnitude increase in Nafion ionic conductivity at a given organic saturation upon introduction of water (Figure 5b).

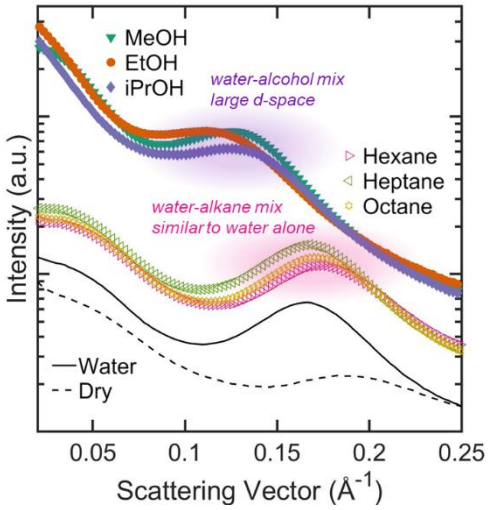

Figure 7: SAXS profiles of Nafion equilibrated with saturated water vapor and saturated methanol (teal triangles), ethanol (orange circles), isopropanol (purple diamonds), hexane (pink right arrows), heptane (green left arrows), and octane (yellow hexagrams). Profiles of Nafion dry (dashed line) and equilibrated with water vapor only (solid line) are included for reference.

Conclusions

The findings presented here show that the well-established hydration-structure-property relationships are fundamentally different in Nafion when swollen with organic sorbates. In organic-swollen Nafion, the sorbate polarity plays a key role in determining the bulk swelling and ionomer domain structure likely based on the solvation tendencies of the sorbate towards the fluoropolymer. In general, more polar solvents produced larger ionomer domains at lower sorbate content and yielded a higher conductivity ionomer. In the presence of water and organic species, water plays a crucial role in the ionomer network formation while alcohols may aid bulk and ionomer-domain swelling by penetrating across the fluoropolymer/water interface. Alkanes showed almost no sorption and therefore minimal impact on ionic conductivity or domain structure regardless of the water content. These results point to fundamental physical relationships between sorbate polarity, ionomer nanostructure, and key ionomer performance metrics which may limit the applicability of PFSAs for electrochemical systems employing alcohols and other polar organic species, while also providing guidance for design of different ionomer-solvent systems for applications involving electro-organic reactions.

Materials

Nafion 117 and Nafion D2021 were purchased from The Fuel Cell Store (College Station, TX). All other chemicals were purchased from Sigma-Aldrich, Inc. (St. Louis, MO).

Experimental

Concise experimental information is included here. A full expanded description of all experimental procedures and calculations can be found in the supporting information.

For ionic conductivity and sorbate uptake experiments, sorbate saturation was controlled by mixing dry and sorbate-saturated nitrogen streams at controlled flow rates. The sorbate-saturated stream was generated by flowing nitrogen through a midget impinger bubbler (Ace Glass) filled with the species of interest. The sorbate saturation s_A can be approximated as:

$$s_A = \frac{\dot{v_a}}{\dot{v_a} + \dot{v}_0} \qquad \text{(Equation 1)}$$

where $\dot{v_a}$ and $\dot{v}_0$ are the flow rates of sorbate-saturated and dry nitrogen, respectively. The total flow rate was maintained at 200 sccm. For mixed sorbate (*i.e.*, organic and water) experiments, the nitrogen stream was replaced with a water-saturated stream and saturation of each species was determined as described above, assuming no interaction between sorbates in the vapor phase.

Sorbate Uptake

ATR-FTIR spectra were collected with a Nicolet 6700 FTIR from Thermo Scientific with Smart iTR attachment and ZnSe single-pass crystal (Thermo Electron North America, West Palm Beach, FL) as the average of 50 spectra collected from 650 – 4000 cm^{-1}. After background collection under nitrogen flow, Nafion films were drop-cast on the crystal from Nafion 2021 to produce a film with thickness > 200 μm, much greater than the expected light penetration depth into Nafion (on the order of 1 μm, dependent on the light wavelength and Nafion refractive index). After drying films at ambient conditions for 30 min and under vacuum for 2 hours, residual alcohol was detected in the ATR-FTIR spectra that persisted under

vacuum and/or nitrogen flow. This residual alcohol was fully removed by rehydrating the films with deionized water for 20 min and then drying again under vacuum. After the final drying step, the ATR crystal was loaded into the FTIR in a custom-built PTFE cell with flow inlet and outlet. At each saturation setpoint, ATR-FTIR spectra were collected periodically until the difference in absorption at a given wavenumber deviated by less than 1% over a 30-minute interval. Plotted points represent final measured values.

Sorbate uptake at intermediate (between 0 and 1) vapor saturation was estimated by linear regression of the as-saturated Nafion ATR-FTIR spectrum to the dry and fully saturated spectra. Relative uptake of sorbate A (X_A) was defined as the dependent variable and the measured absorbance at each wavenumber A_j, where subscript j is the index for each wavenumber, as the independent variable. 12,238 wavenumbers were evaluated in the range 3600 to 650 cm^{-1}. Relative sorbate uptake X_A was defined as

$$X_A = a + \sum_{j=1}^{12238} b_j A_j \qquad \text{(Equation 2)}$$

where b_j is a weighted fitting parameter describing the sensitivity of A_j to sorbate A saturation at the j^{th} wavenumber, and a is an additional fitting parameter. Mass fraction of sorbate in the ionomer was calculated as

$$m_A = X_A\left(\frac{\Delta M}{M_{dry} + \Delta M}\right) \qquad \text{(Equation 3)}$$

where m_A is the mass fraction of species A and M_{dry} and ΔM are the initial (dry) mass and mass uptake of sorbate, respectively, determined by gravimetric dynamic vapor sorption. This method offers several key advantages over traditional absorbance-based analysis techniques (*i.e.* Beer's Law at a fixed wavenumber or linear combination of the absorbance spectra of individual components) as it (*i*) accounts for changes in Nafion and sorbate spectra upon mixing (*ii*) uses the entire absorbance range and (*iii*) enables simple analysis of multi-sorbate mixtures. In cases with multiple sorbates, a multi-target linear regression was performed using the spectra of dry Nafion and Nafion saturated with each sorbate. Relative uptake X_i of each sorbate was estimated as

$$X_i = a_i + \sum_{j=1}^{12238} b_{ij} A_j \quad \text{(Equation 4)}$$

where subscript i denotes the sorbate. The linear regression was performed using Scikit-learn in Python[47]. Demonstration of ATR-FTIR and regression results for methanol-equilibrated Nafion can be found in the supporting information.

Ionic Conductivity

Nafion ionic conductivity was measured using a BT-110 four probe in-plane membrane conductivity clamp (Scribner Associates, Inc., Southern Pines, NC). A strip of Nafion 117 was cut to a width ~ 1 cm and long enough to completely cover two platinum-gauze force leads (2.5 cm). Membrane width was measured from photographs of the membrane in ImageJ by length-calibrated pixel count, with at least 20 measurements per membrane. Dry thickness of Nafion 117 is reported as 183 μm and was verified by micrometer measurement prior to affixing in the conductivity clamp. The conductivity clamp was placed in a vented environmental chamber with flow inlet.

Sorbate saturation was incremented from 0 to 1 in steps of 0.125. The membrane was equilibrated at each step for 2 hours or until the difference in conductivity values deviated by less than 0.1% over a 10-min interval. Mixed-sorbate experiments were started at full organic saturation (water saturation of 0) and the organic saturation was decremented as the water saturation was incremented.

Conductivity was determined by linear-sweep voltammetry from -0.1 to 0.1 V at a sweep rate of 20 mV s^{-1}. Cell resistance R was determined from the slope of the LSV trace and conductivity was calculated as

$$\kappa = \frac{L}{Rwt} \quad \text{(Equation 5)}$$

Where L is the distance between the counter- and working- sense leads, R is the cell resistance, and w and t are the width and thickness of the dry membrane scaled by the linear swelling ε at the given saturation step

$$\varepsilon = s_A(1 + \frac{\Delta V}{V_{dry}})^{\frac{1}{3}} \quad \text{(Equation 6)}$$

where $\frac{\Delta V}{V_{dry}}$ is the volumetric expansion of Nafion 117 saturated with sorbate A as determined by ATR-FTIR regression at the same saturation. Conductivity was measured every 10 minutes during vapor equilibration until the deviation between measurements was less than 0.1%.

Small Angle X-Ray Scattering

SAXS measurements were performed at beamline 7.3.3 of the Advanced Light Source at Lawrence Berkeley National Lab. The X-ray energy was 10 keV with a monochromator resolution E/dE of 100. Scattering patterns were acquired with a 2D Dectris Pilatus 1M CCD area detector (172 μm x 172 μm pixel size). The scattering wave vector, $q = 4\pi \sin\left(\frac{\theta}{2}\right)/\lambda$, where θ is the scattering angle, was in the range of 0.004 to 0.4 $Å^{-1}$. Experiments were conducted *in-situ* by equilibrating the membrane samples in liquid or in vapor using custom-designed sealed sample holders with X-ray transparent Kapton™ windows for imaging. For liquid-equilibrated experiments, circular membrane samples were completely immersed in the holder filled with liquid (water or alcohol). Vapor-equilibration of the samples was accomplished using sealed holders containing a controlled mixture of water and solvent in the solution reservoir. For each equilibrium method, samples were equilibrated for at least 2 hours and SAXS images for vapor- and liquid-equilibrated samples were collected *in-situ* with an exposure time of 20 seconds. The collected two-dimensional scattering patterns were azimuthally integrated to generate 1-D intensity profiles, *I(q)*, which were corrected for background scattering. From the SAXS data, hydrophilic-domain spacing and full-width at half-maximum (*FWHM*), were calculated using a Gaussian fit to the ionomer scattering peak.

Supporting Information

Sorbate Mass, Molar, and Volume Uptake. ATR-FTIR Spectra Collection. ATR-FTIR Spectral Regression. Ionic Conductivity. Small Angle X-Ray Scattering.

Acknowledgements

A. Kusoglu acknowledges the funding from the U.S. Department of Energy Hydrogen and Fuel Cell Technologies Office (HFTO) (Contract No. DE-AC02-05CH11231). This work also made use of facilities at the Advanced Light Source Beamline 7.3.3, supported by the Office of Science, Office of Basic Energy Sciences, of the U.S. Department of Energy (Contract No. DE-AC02-05CH11231). The authors would like to acknowledge the financial support of the National Science Foundation and NYU Tandon School of Engineering through M. A. M. startup fund. This material is based upon work supported by the National Science Foundation under Grant No. 1943972.

Author Information

[+]present address: Lawrence Berkeley National Laboratory, Berkeley, CA 94720

References

(1) Mauritz, K. A.; Moore, R. B. State of Understanding of Nafion. *Chem. Rev.* **2004**, *104* (10), 4535–4585. https://doi.org/10.1021/cr0207123.

(2) Kusoglu, A.; Weber, A. Z. New Insights into Perfluorinated Sulfonic-Acid Ionomers. *Chem. Rev.* **2017**, *117* (3), 987–1104. https://doi.org/10.1021/acs.chemrev.6b00159.

(3) Ayers, K.; Danilovic, N.; Ouimet, R.; Carmo, M.; Pivovar, B.; Bornstein, M. Perspectives on Low-Temperature Electrolysis and Potential for Renewable Hydrogen at Scale. *Annu. Rev. Chem. Biomol. Eng.* **2019**, *10*, 219–239. https://doi.org/10.1146/annurev-chembioeng-060718-030241.

(4) Kushner, D. I.; Crothers, A. R.; Kusoglu, A.; Weber, A. Z. Transport Phenomena in Flow Battery Ion-Conducting Membranes. *Curr. Opin. Electrochem.* **2020**, *21*, 132–139.

(5) Allen, F. I.; Comolli, L. R.; Kusoglu, A.; Modestino, M. A.; Minor, A. M.; Weber, A. Z. Morphology of Hydrated As-Cast Nafion Revealed through Cryo Electron Tomography. *ACS Macro Lett.* **2015**, *4* (1), 1–5. https://doi.org/10.1021/mz500606h.

(6) Grot, W. Discovery and Development of Nafion Perfluorinated Membranes. *Chem. Ind.* **1985**, 647–649.

(7) Grot, W. G. Polymerization of Fluorinated Copolymers. 5,281,680, 1994.

(8) Hahn, C.; Jaramillo, T. F.; Weber, A. Z.; Higgins, D.; Xiang, C. Gas-Diffusion Electrodes for Carbon Dioxide Reduction: A New Paradigm. *ACS Energy Lett.* **2019**, *4*, 317–324. https://doi.org/10.1021/acsenergylett.8b02035.

(9) Pătru, A.; Binninger, T.; Pribyl, B.; Schmidt, T. J. Design Principles of Bipolar Electrochemical

Co-Electrolysis Cells for Efficient Reduction of Carbon Dioxide from Gas Phase at Low Temperature. *J. Electrochem. Soc.* **2019**, *166* (2), F34–F43. https://doi.org/10.1149/2.1221816jes.

(10) Weekes, D. M.; Salvatore, D. A.; Reyes, A.; Huang, A.; Berlinguette, C. P. Electrolytic CO2 Reduction in a Flow Cell. *Acc. Chem. Res.* **2018**, *51*, 910–918. https://doi.org/10.1021/acs.accounts.8b00010.

(11) Verma, S.; Lu, S.; Kenis, P. J. A. Co-Electrolysis of CO2 and Glycerol as a Pathway to Carbon Chemicals with Improved Technoeconomics Due to Low Electricity Consumption. *Nat. Energy* **2019**, *4* (June), 466–474. https://doi.org/10.1038/s41560-019-0374-6.

(12) Wasmus, S.; Kuver, A. Methanol Oxidation and Direct Methanol Fuel Cells : A Selective Review. *J. Electroanal. Chem.* **1999**, *461*, 14–31.

(13) Neburchilov, V.; Martin, J.; Wang, H.; Zhang, J. A Review of Polymer Electrolyte Membranes for Direct Methanol Fuel Cells. *J. Power Sources* **2007**, *169*, 221–238. https://doi.org/10.1016/j.jpowsour.2007.03.044.

(14) Jorissen, L.; Gogel, V.; Kerres, J.; Garche, J. New Membranes for Direct Methanol Fuel Cells. *J. Power Sources* **2002**, *105*, 267–273.

(15) Blanco, D. E.; Prasad, P. A.; Dunningan, K.; Modestino, M. A. Insights into Membrane-Separated Organic Electrosynthesis: The Case of Adiponitrile Electrochemical Production. *React. Chem. Eng.* **2020**, *5* (1), 136–144. https://doi.org/10.1039/c9re00389d.

(16) Jing, Y.; Wu, M.; Wong, A. A.; Fell, E. M.; Jin, S.; Pollack, D. A.; Kerr, E. F.; Gordon, R. G.; Aziz, M. J. In Situ Electrosynthesis of Anthraquinone Electrolytes in Aqueous Flow Batteries. *Green Chem.* **2020**, *22*, 6084–6092. https://doi.org/10.1039/d0gc02236e.

(17) Pletcher, D.; Green, R. A.; Brown, R. C. D. Flow Electrolysis Cells for the Synthetic Organic Chemistry. *Chem. Rev.* **2018**, *118*, 4573–4591. https://doi.org/10.1021/acs.chemrev.7b00360.

(18) Voskian, S.; Hatton, T. A. Faradaic Electro-Swing Reactive Adsorption for CO2 Capture. *Energy Environ. Sci.* **2019**, *12* (12), 3530–3547. https://doi.org/10.1039/c9ee02412c.

(19) Kusoglu, A.; Savagatrup, S.; Clark, K. T.; Weber, A. Z. Role of Mechanical Factors in Controlling the Structure-Function Relationship of PFSA Ionomers. *Macromolecules* **2012**, *45* (18), 7467–7476. https://doi.org/10.1021/ma301419s.

(20) Zhao, Q.; Carro, N.; Ryu, H. Y.; Benziger, J. Sorption and Transport of Methanol and Ethanol in H+-Nafion. *Polymer (Guildf).* **2012**, *53*, 1267–1276. https://doi.org/10.1016/j.polymer.2012.01.050.

(21) Saito, M.; Tsuzuki, S.; Hayamizu, K.; Okada, T. Alcohol and Proton Transport in Perfluorinated Ionomer Membranes for Fuel Cells. *J. Phys. Chem. B* **2006**, *110* (48), 24410–24417. https://doi.org/10.1021/jp0643496.

(22) Berens, S. J.; Yahya, A.; Fang, J.; Angelopoulos, A.; Nickels, J. D.; Vasenkov, S. Transition between Different Diffusion Regimes and Its Relationship with Structural Properties in Nafion by High Field Diffusion NMR in Combination with Small-Angle X-ray and Neutron Scattering. *J. Phys. Chem. B* **2020**, *124*, 8943–8950. https://doi.org/10.1021/acs.jpcb.0c07249.

(23) Randová, A.; Bartovská, L.; Hovorka, Š.; Friess, K.; Izák, P. The Membranes (Nafion and LDPE) in Binary Liquid Mixtures Benzene + Methanol - Sorption and Swelling. *Eur. Polym. J.* **2009**, *45* (10), 2895–2901. https://doi.org/10.1016/j.eurpolymj.2009.06.023.

(24) Welch, C.; Labouriau, A.; Hjelm, R.; Orler, B.; Johnston, C.; Kim, Y. S. Nafion in Dilute Solvent Systems: Dispersion or Solution? *ACS Macro Lett.* **2012**, *1* (12), 1403–1407. https://doi.org/10.1021/mz3005204.

(25) Abroshan, H.; Akbarzadeh, H.; Taherkhani, F. Effect of Water – Methanol Content on the Structure of Nafion in the Sandwich Model and Solvent Dynamics in Nano-Channels ; a Molecular Dynamics Study. **2011**, *8976*. https://doi.org/10.1080/00268976.2010.549846.

(26) Zhao, Q.; Carro, N.; Ryu, H. Y.; Benziger, J. Sorption and Transport of Methanol and Ethanol in H+ -Nafion. *Polymer (Guildf).* **2012**, *53*, 1267–1276. https://doi.org/10.1016/j.polymer.2012.01.050.

(27) Hallinan, D. T.; Elabd, Y. A. Diffusion and Sorption of Methanol and Water in Nafion Using Time-Resolved Fourier Transform Infrared - Attenuated Total Reflectance Spectroscopy. *J. Phys. Chem. B* **2007**, *111*, 13221–13230. https://doi.org/10.1021/jp075178n.

(28) Affoune, A. M.; Yamada, A.; Umeda, M. Conductivity and Surface Morphology of Nafion Membrane in Water and Alcohol Environments. *J. Power Sources* **2005**, *148* (1–2), 9–17. https://doi.org/10.1016/j.jpowsour.2005.01.039.

(29) Jung, B.; Moon, H.; Nathaniel, G.; Baro, B. Effect of Methanol on Plasticization and Transport Properties of a Perfluorosulfonic Ion-Exchange Membrane. **2011**, *196*, 1880–1885. https://doi.org/10.1016/j.jpowsour.2010.09.030.

(30) Kreuer, K. D.; Portale, G. A Critical Revision of the Nano-Morphology of Proton Conducting Ionomers and Polyelectrolytes for Fuel Cell Applications. *Adv. Funct. Mater.* **2013**, *23* (43), 5390–5397. https://doi.org/10.1002/adfm.201300376.

(31) Hickner, M. A. Water-Mediated Transport in Ion-Containing Polymers. *J. Polym. Sci. Part B Polym. Phys.* **2012**, *50* (1), 9–20. https://doi.org/10.1002/polb.22381.

(32) Rollet, A. L.; Diat, O.; Gebel, G. A New Insight into Nafion Structure. *J. Phys. Chem. B* **2002**, *106* (12), 3033–3036. https://doi.org/10.1021/jp020245t.

(33) Schmidt-Rohr, K.; Chen, Q. Parallel Cylindrical Water Nanochannels in Nafion Fuel-Cell Membranes. *Mater. Sustain. Energy A Collect. Peer-Reviewed Res. Rev. Artic. from Nat. Publ. Gr.* **2010**, 238–246. https://doi.org/10.1142/9789814317665_0033.

(34) Gierke, T. D.; Munn, G. E.; Wilson, F. C. The Morphology in Nafion Perfluorinated Membrane Products, as Determined by Wide- and Small-Angle x-Ray Studies. *J. Polym. Sci. Polym. Phys. Ed.* **1981**, *19* (11), 1687–1704. https://doi.org/10.1002/pol.1981.180191103.

(35) Hsu, W. Y.; Gierke, T. D. Ion Transport and Clustering in Nafion Perfluorinated Membranes. *J. Memb. Sci.* **1983**, *13* (3), 307–326. https://doi.org/10.1016/S0376-7388(00)81563-X.

(36) Gebel, G.; Lambard, J. Small-Angle Scattering Study of Water-Swollen Perfluorinated Ionomer Membranes. *Macromolecules* **1997**, *30* (25), 7914–7920. https://doi.org/10.1021/ma970801v.

(37) Kusoglu, A.; Modestino, M. A.; Hexemer, A.; Segalman, R. A.; Weber, A. Z. Subsecond Morphological Changes in Nafion during Water Uptake Detected by Small-Angle X-Ray Scattering. *ACS Macro Lett.* **2012**, *1* (1), 33–36. https://doi.org/10.1021/mz200015c.

(38) Roche, E. J.; Pineri, M.; Duplessix, R. Phase Separation in Perfluorosulfonate Ionomer Membranes. *J. Polym. Sci. Part A-2, Polym. Phys.* **1982**, *20* (1), 107–116. https://doi.org/10.1002/pol.1982.180200109.

(39) Fujimura, M.; Hashimoto, T.; Kawai, H. Small-Angle X-Ray Scattering Study of Perfluorinated Ionomer Membranes. 2. Models for Ionic Scattering Maximum. *Macromolecules* **1982**, *15* (1), 136–144. https://doi.org/10.1021/ma00229a028.

(40) Su, G. M.; Cordova, I. A.; Yandrasits, M. A.; Lindell, M.; Feng, J.; Wang, C.; Kusoglu, A. Chemical and Morphological Origins of Improved Ion Conductivity in Perfluoro Ionene Chain Extended Ionomers. *J. Am. Chem. Soc.* **2019**, *141* (34), 13547–13561. https://doi.org/10.1021/jacs.9b05322.

(41) Berrod, Q.; Lyonnard, S.; Guillermo, A.; Ollivier, J.; Frick, B.; Manseri, A.; Améduri, B.; Gébel, G. Nanostructure and Transport Properties of Proton Conducting Self-Assembled Perfluorinated Surfactants: A Bottom-Up Approach toward PFSA Fuel Cell Membranes. *Macromolecules* **2015**, *48* (17), 6166–6176. https://doi.org/10.1021/acs.macromol.5b00770.

(42) Loppinet, B.; Gebel, G.; Williams, C. E. Small-Angle Scattering Study of Perfluorosulfonated Ionomer Solutions. *J. Phys. Chem. B* **1997**, *101* (10), 1884–1892. https://doi.org/10.1021/jp9623047.

(43) Rivin, D.; Kendrick, C. E.; Gibson, P. W.; Schneider, N. S. Solubility and Transport Behavior of Water and Alcohols in Nafion. *Polymer (Guildf).* **2001**, *42*, 623–635.

(44) Gebel, G.; Aldebert, P.; Pineri, M. Swelling Study of Perfluorosulphonated Ionomer Membranes. *Polymer (Guildf).* **1993**, *34* (2), 333–339. https://doi.org/10.1016/0032-3861(93)90086-P.

(45) Blanco, D. E.; Modestino, M. A. Organic Electrosynthesis for Sustainable Chemical Manufacturing. *Trends Chem.* **2019**, *1* (1), 8–10. https://doi.org/10.1016/j.trechm.2019.01.001.

(46) Baker, A. M.; Crothers, A. R.; Chintam, K.; Luo, X.; Weber, A. Z.; Borup, R. L.; Kusoglu, A. Morphology and Transport of Multivalent Cation-Exchanged Ionomer Membranes Using Perfluorosulfonic Acid–CeZ+ as a Model System. *ACS Appl. Polym. Mater.* **2020**, *2* (8), 3642–3656. https://doi.org/10.1021/acsapm.0c00633.

(47) Pedregosa, F.; Varoquaux, G.; Gramfort, A.; Michel, V.; Thirion, B.; Grisel, O.; Blondel, M.; Prettenhofer, P.; Weiss, R.; Dubourg, V.; et al. Scikit-Learn: Machine Learning in Python. *J. Mach. Learn. Res.* **2011**, *12*, 2825–2830.